HHS Public Access

Author manuscript

J Med Genet. Author manuscript; available in PMC 2018 January 16.

Published in final edited form as:

J Med Genet. 2016 August ; 53(8): 568–574. doi:10.1136/jmedgenet-2016-103756.

Identification of biallelic *LRRK1* mutations in osteosclerotic metaphyseal dysplasia and evidence for locus heterogeneity

Aritoshi Iida[1], **Weirong Xing**[2,3], **Martine K F Docx**[4], **Tomoki Nakashima**[5,6], **Zheng Wang**[1,7], **Mamori Kimizuka**[8], **Wim Van Hul**[9], **Dietz Rating**[10], **Jürgen Spranger**[11], **Hirohumi Ohashi**[12], **Noriko Miyake**[13], **Naomichi Matsumoto**[13], **Subburaman Mohan**[2,3], **Gen Nishimura**[14], **Geert Mortier**[9], and **Shiro Ikegawa**[1,8]

[1]Laboratory for Bone and Joint Diseases, RIKEN Center for Integrative Medical Sciences, Tokyo, Japan

[2]Musculoskeletal Disease Center, Jerry L Pettis Memorial VA Medical Center, Loma Linda, California, USA

[3]Department of Medicine, Loma Linda University, Loma Linda, California, USA

[4]Department of Paediatric Chronic Diseases and Nephrology, Queen Paola Children's Hospital, Antwerp, Belgium

[5]Department of Cell Signaling, Graduate school of Medical and Dental Science, Tokyo Medical and Dental University, Tokyo, Japan

[6]Japan Science and Technology Agency, PRESTO, Tokyo, Japan

[7]State Key Laboratory of Medical Molecular Biology, McKusick-Zhang Center for Genetic Medicine and Institute of Basic Medical Sciences, Chinese Academy of Medical Sciences & Peking Union Medical College, Beijing, China

[8]Department of Orthopaedics, National Rehabilitation Center for Disabled Children, Tokyo, Japan

[9]Department of Medical Genetics, University of Antwerp and Antwerp University Hospital, Edegem, Belgium

[10]Department of Pediatrics, St Annastiftskinderkrankenhaus, Ludwigshafen, Germany

[11]Centre for Pediatrics and Adolescent Medicine, Freiburg, Germany

Correspondence to: Professor Shiro Ikegawa, Laboratory for Bone and Joint Diseases, RIKEN Center for Integrative Medical Sciences, 4-6-1 Shirokane-dai, Minatoku, Tokyo 108-8639, Japan; sikegawa@ims.u-tokyo.ac.jp or Professor Geert Mortier, Department of Medical Genetics, University of Antwerp and Antwerp University Hospital, Edegem 2650, Belgium; geert.mortier@uantwerpen.be.

AI and WX contributed equally.

Contributors

SI designed the project and provided overall project management. AI, GM and SI wrote the paper. AI performed the sequence experiments and analysed the data. WX and SM generated *LRRK1*-deficient mice and analysed the data. TN and ZW performed the experiments and analysed the data. MKFD, MK, WVH, DR, JS, HO and GM collected and managed the DNA samples. NoM and NaM performed the exome experiments and analysed the data. GN analysed the clinical data.

Competing interests None declared.

Patient consent Obtained.

Ethics approval This study was performed with the approval of the ethical committees of RIKEN and participating institutions.

Provenance and peer review Not commissioned; externally peer reviewed.

[12]Division of Medical Genetics, Saitama Children's Medical Center, Saitama, Japan

[13]Department of Human Genetics, Yokohama City University Graduate School of Medicine, Yokohama, Japan

[14]Department of Pediatric Imaging, Tokyo Metropolitan Children's Medical Center, Fuchu, Japan

Abstract

Background—Osteosclerotic metaphyseal dysplasia (OSMD) is a unique form of osteopetrosis characterised by severe osteosclerosis localised to the bone ends. The mode of inheritance is autosomal recessive. Its genetic basis is not known.

Objective—To identify the disease gene for OSMD.

Methods and results—By whole exome sequencing in a boy with OSMD, we identified a homozygous 7 bp deletion (c.5938_5944delGAGTGGT) in the *LRRK1* gene. His skeletal phenotype recapitulated that seen in the *Lrrk1*-deficient mouse. The shared skeletal hallmarks included severe sclerosis in the undermodelled metaphyses and epiphyseal margins of the tubular bones, costal ends, vertebral endplates and margins of the flat bones. The deletion is predicted to result in an elongated LRRK1 protein (p.E1980Afs*66) that lacks a part of its WD40 domains. In vitro functional studies using osteoclasts from *Lrrk1*-deficient mice showed that the deletion was a loss of function mutation. Genetic analysis of *LRRK1* in two unrelated patients with OSMD suggested that OSMD is a genetically heterogeneous condition.

Conclusions—This is the first study to identify the causative gene of OSMD. Our study provides evidence that *LRRK1* plays a critical role in the regulation of bone mass in humans.

INTRODUCTION

Osteosclerotic metaphyseal dysplasia (OSMD; OMIM %615198) is a unique form of osteopetrosis characterised by a distinctive pattern of osteosclerosis (localised increase of bone density).[1,2] Only five patients in four families have been reported.[2–5] The clinical features include developmental delay, hypotonia and seizures.[2–5] Osteosclerosis localises predominantly to the metaphyses and epiphyseal margins of the appendicular bones and metaphyseal equivalents of the axial bones. The metaphyses show wide sclerotic bands and undermodelling, whereas the diaphyses are not sclerotic or even osteopenic. Osteosclerosis is also seen in the vertebral endplates, costal ends and margins of the flat bones. The skull is not affected. Laboratory abnormalities include raised levels of serum alkaline phosphatase (ALP), aspartate aminotransferase and creatine kinase and increased urinary pyridinoline and deoxypyridinoline excretion.[2–5] An autosomal recessive inheritance has been suggested based on the occurrence in siblings born to first-cousin parents[2]; however, the disease gene has not yet been found.

To identify the disease gene for OSMD, we recruited three unrelated individuals diagnosed with OSMD and performed molecular genetic studies.

MATERIALS AND METHODS

Patients

Three patients (P1–3; see online supplementary table S1) diagnosed as having OSMD by experts of skeletal dysplasia (GN and GM) based on their clinical and radiographic findings were included in the study. P2 has been previously reported.[2] P1 and P2 were consanguineous. The study protocol was approved by the ethical committee of RIKEN and participating institutions. Peripheral blood was obtained from the patients and their family members after informed consent and was used for the study.

Exome sequencing and variant calling

Genomic DNA was extracted by standard procedures from peripheral blood or Epstein–Barr virus immortalised lymphocytes. Concentration of DNAs for whole exome sequencing was measured using a Qubit V.2.0 Fluorometer (Life Technologies, Carlsbad, California, USA). Whole exome sequencing was performed as previously described.[67] Briefly, DNA (3 μg) was sheared by Covaris S2 system (Covaris, Wobum, Massachusetts, USA) and processed by SureSelectXT Human All Exon V5 (Agilent Technologies, Santa Clara, California, USA). Captured DNA was sequenced using HiSeq 2000 (Illumina, San Diego, California, USA) with 101 bp pair-end reads with seven indices. Image analysis and base calling were performed using HiSeq Control Software/Real-time analysis and CASAVA 1.8.2 (Illumina). Reads were mapped to the reference human genome (hg19) by Novoalign-3.02.04. Aligned reads were processed by Picard to remove PCR duplicates. Variants were called by Genome Analysis Toolkit (GATK) v2.7-4 based on GATK Best Practice Workflow v3 and annotated by ANNOVAR (downloaded at 2013 June).

PCR and Sanger sequencing

We performed Sanger sequencing to confirm the deletion identified in the patient and parents by the exome sequencing. We amplified exon 34 by PCR using primers, *LRRK1*fsFP1 (forward primer): 5′-TTAGCCAGCTCCGCCTTCCT-3′ and *LRRK1*fsRP1 (reverse primer): 5′-TCCTTGGAGAACTAGA GGCCGAT-3′ and sequenced both strands. We also designed the primer sets to amplify all exons of *LRRK1* and performed mutation screening for the subjects in whom *LRRK1* mutation was not identified by the whole genome sequencing. Sanger sequencing was performed on a 3730 DNA analyzer (Life Technologies). Sequencher V.4.7 (Gene Codes, Michigan, USA) and Genetyx (Genetyx Inc, Tokyo, Japan) were used for aligning sequencing chromatographs to reference sequences and mutation detection.

Evaluation of the deletion found in *LRRK1*

We evaluated the deletion by databases, dbSNP (http://www.ncbi.nlm.nih.gov/projects/SNP/), 1000 genomes (http://www.1000genomes.org/), Human Gene Mutation Database (https://portal.biobase-international.com/hgmd/pro/start.php) and ESP6500 (http://evs.gs.washington.edu/EVS/).

Homozygosity mapping

Homozygosity mapping was performed using Homozygosity-Mapper as previously described[8] on whole exome sequencing data of P1 and P2.

In vitro osteoclastogenesis and collection of osteoblast- and osteocyte-rich fractions

In vitro osteoclastogenesis was performed as described previously.[9] Briefly, mouse bone marrow cells were cultured with 10 ng/mL macrophage colony stimulating factor (M-CSF) (R&D Systems, Minnesota, USA) for 2 days and bone marrow-derived monocyte/macrophage precursor cells (BMMs) were obtained. BMMs were cultured with 25 ng/mL receptor activator of nuclear factor κ-B ligand (RANKL) (PeproTech, Rocky Hill, New Jersey, USA) and M-CSF for 3 days. Osteoclastogenesis was evaluated by tartrate-resistant acid phosphatase (TRAP) staining using leucocyte acid phosphatase staining kit from Sigma (386-A). The staining mixture contained citrate, tartrate, acetate and naphthol AS-BI phosphoric acid solutions. The multinucleated cells (number of nuclei ≥3) were stained for 5–10 min at 37°C, then washed three times with phosphate-buffered saline. TRAP-positive multinucleated cells were counted. Osteoblast- and osteocyte-rich fractions were collected as described previously.[10]

Quantitative RT-PCR analysis

Total RNA was extracted using ISOGEN (Nippon Gene, Tokyo, Japan) following the manufacturer's protocol. Real-time quantitative RT-PCR analysis was performed as described previously.[911] Briefly, first-strand cDNAs were synthesised from 0.5 μg of total RNA using Superscript III RT (Life Technologies). Quantitative RT-PCR analysis was performed with the CFX384 Touch real-time system (Bio-Rad Laboratories, Hercules, California, USA) using SYBR Green real-time PCR master mix (Toyobo, Osaka, Japan). The relative gene expression levels were calculated using the Ct method after the values were normalised against *Gapdh* expression. The primer sequences used in real-time RT-PCR analysis were: *Gapdh*, 5′-GGATGCAGGGATGATGTTCT-3′ and 5′-AACTTTGCCATTGTGGAAGG-3′; *Ctsk*, 5′-GGGAAGCAAGCACTGGATAA-3′ and 5′-CCGAGCCAAGAGAGCATATC-3′; *Nfatc1*, 5′-CAAGTCTCACCACAGGGCTCACTA-3′ and 5′-GCGTGAGAGGTTCATTCTCCAAGT-3′; *Lrrk1*, 5′-GAACTGAGCATGACCTGAGC-3′ and 5′-TCCTCCATGTCTAGGAACCC-3′; *Dmp1*, 5′-GGTTTTGACCTTGTGGGAAA-3′ and 5′-TTGGGATGCGATTCCTCTAC-3′.

Viral plasmid construction and lentivirus generation

Lentiviral plasmid of pSSFV-*LRRK1* was generated by replacing green fluorescent protein (GFP) with a synthesised 3xFLAG/*LRRK1* DNA (GenScript, Piscataway, New Jersey, USA) at the restriction sites of *Sgf*I and *Pme*I of the pRRLsin-cPPT-SFFV-GFP-wpre vector. Lentiviral pSSFV-*LRRK1*-WDmt vector was generated by subcloning a synthesised mutated WD40 DNA fragment into the restriction sites of *Bsr*GI and Pmel of the pSSFV-*LRRK1*. Lentiviral particles were generated by co-transfection of pSSFV-*LRRK1* or pSSFV-*LRRK1*-WDmt with Pax2 and VSVG plasmids in 293T cells. Lentiviral productions were generated by transfection in 293T cells as described previously.[12] Forty-eight hours after transfection, culture supernatants containing viral particles were collected, spun at 2000×*g*

for 10 min and filtered through a 0.45 mm filter. Titres were determined by infecting 293T cells with serial dilutions and examining GFP expression of infected cells 24 h after infection. Primary monocytes derived from mouse bone marrow were seeded on bone slices in 48-well plates at a density of 10 000 cells/well and transduced by adding viral supernatant at a multiplicity of infection (MOI) of 5 in the presence of polybrene (8 mg/mL) and M-CSF (20 ng/mL) for 24 h, followed by replacement of a fresh osteoclast differentiation medium containing M-CSF (20 ng/mL) and RANKL (30 ng/mL).

In vitro osteoclast formation and bone resorption pit assays

Primary osteoclast precursors were isolated from the spleen or bone marrow of femur and tibia from 5-week-old mice as described previously.[13] The isolated precursors were maintained in α-minimal essential medium supplemented with 10% fetal bovine serum, penicillin (100 units/mL), streptomycin (100 μg/ mL) and M-CSF (20 ng/mL) at 37°C in 5% CO_2 for 3 days to stimulate monocyte proliferation. To induce osteoclast differentiation, trypsinised precursors were seeded in 48-well plates (5000 cells/well) and incubated with M-CSF (20 ng/mL) and RANKL (30 ng/mL). The medium was changed every 2 days. Osteoclastogenesis was evaluated by counting TRAP staining-positive multinucleated cells having at least three nuclei. Osteoclast precursors were differentiated in vitro for 9 days until formation of large multinuclear cells for TRAP staining. Parallel cultures were maintained in osteoclast differentiation medium for another 4 days for pit staining. For bone resorption pit assays, slices from bovine cortical bone were placed in 48-well plates and cells were differentiated on top of the bone slices as described above. Cells on bone slices were digested with trypsin at 37°C overnight. Multinucleated cells were further removed by 5 min sonication in 1 M ammonia. Air-dried bone slices were stained with haematoxylin. The entire surface of each bone slice was examined and the total resorbed area per bone slice was quantified using ImageJ software (National Institutes of Health, USA).

RESULTS

Identification of a *LRRK1* mutation in a patient with OSMD

We conducted whole exome sequencing in two probands (P1 and P2) (see online supplementary table S1) and obtained about 2.4–2.5 Gb sequences, which were successfully mapped to all human RefSeq. For both samples, at least 95.4% of all coding regions were covered in a depth of 10 reads (see online supplementary table S2). No common candidate genes that displayed mutations in the two subjects were found; however, we identified a homozygous 7 bp deletion (c.5938_5944delGAGTGGT) in the last exon of *LRRK1* (leucine-rich repeat kinase 1) in P1. The deletion was not deposited in any databases, including dbSNP, 1000 genomes, Human Gene Mutation Database and ESP6500. The homozygosity mapping using the whole exome sequencing data in P1 and the parents showed that *LRRK1* is residing in a 2.4 Mb homozygous region of the patient genome (see online supplementary table S3). The 7 bp deletion was confirmed by Sanger sequencing (figure 1A). The parents were heterozygous for the deletion.

Characterisation of the *LRRK1* mutation

Human *LRRK1* was first identified as a gene encoding a related protein of MFH (malignant fibrous histiocytoma)-amplified sequences with leucine-rich tandem repeats, an oncogene promoting tumorigenesis in nude mice.[14] The *LRRK1* gene (NM_024652) consists of 34 exons, encompassing ~150 kb on chromosome 15q26.3. *LRRK1* encodes a 2015 amino acid multidomain protein that contains ankyrin repeats, leucine-rich repeats, Ras of complex proteins (Roc), C-terminal of Roc (COR) and serine threonine kinase domain as well as seven tryptophan-aspartic acid dipeptide (WD) 40 domains at the C-terminus (figure 1B).[15–17] The deletion in P1 is located within the last exon (exon 34) of *LRRK1*. It is predicted to result in a frame shift that destroys the seventh WD40 domain and adds a unique stretch of 66 amino acids to the C-terminal of the *LRRK1* protein (p.E1980Afs*66). The WD40 domain is a ring-like structure that folds into a seven-bladed β propeller and also mediates protein–protein interaction.[18] *Lrrk1* is a mediator in the c-Src signalling pathway in mice and there is evidence that it negatively regulates bone mass.[19] Hence, the partial deletion of WD40 domain of *LRRK1* may abolish the interaction with additional unknown proteins in the c-Src signalling pathway.

Clinical features of the patient with the *LRRK1* mutation

P1 was a 14-month-old boy who presented with failure to thrive, hypotonia and a delay in psychomotor development. Parents were of Moroccan (Berbers) origin and first cousins. He was born at 40 weeks with a birth weight of 3700 g. Physical examination at the age of 14 months did not reveal dysmorphic features but neurological evaluation showed hypotonia with weak deep tendon reflexes. The abdomen was slightly distended, but hepatosplenomegaly was clinically absent. His weight at 14 months was 8400 g (5th centile), his height 72 cm (2nd centile is 73 cm) and his fronto-occipital circumference 48 cm (98th centile). A skeletal survey (figure 2) showed a normal skull and vertebral height. The vertebral endplates, costal ends and iliac margins were sclerotic. Broad sclerotic bands were also seen in the metaphyses of the long and short tubular bones. Bone density was not increased in the diaphyses of the tubular bones. Metaphyseal undermodelling was evident in the proximal femora, distal radii and distal ulnae. Because of the failure to thrive and hypotonia, a metabolic investigation was initiated. This investigation showed normal values for serum amino acids and urinary organic acids but high levels of creatine kinase (31 300 U/L; normal 24–170 U/L), aspartate aminotransferase (649 U/L; normal 20–60 U/L), alanine aminotransferase (295 U/L; normal 19–61 U/L) and lactate dehydrogenase (5075 U/L; normal 425–975 U/L) in blood. ALP was decreased (103 U/L; normal 129–291 U/L). Lead poisoning was excluded by urine analysis. Additionally, a SNP array analysis was performed and showed a deletion (size: 102–113 kb) in the dystrophin gene on Xp21.1. A multiplex ligation-dependent probe amplification analysis confirmed the deletion involving exons 48–50 of the dystrophin gene, which was compatible with the diagnosis of Duchenne muscular dystrophy. The last follow-up at the age of 25 months showed a height of 79.8 cm (P2=82 cm), a weight of 10.8 kg (10th–25th centile) and a head circumference of 50 cm (98th centile). No dysmorphic features were present and the limbs were unremarkable (see online supplementary figure S1A). He had very weak deep tendon reflexes (due to the muscular dystrophy). Radiological examination showed that the metaphyseal sclerotic bands and

marginal sclerosis of the flat bones had become less conspicuous (see online supplementary figures S1B–D).

Phenotype of the *Lrrk1* knockout mice

Lrrk1 knockout (KO) mice have been reported to exhibit severe osteopetrosis.[19] We conducted a detailed skeletal survey and histologic analysis of the *Lrrk1* KO mice and concluded that the bone changes were very similar to those seen in P1 (figure 3). Briefly, the vertebral bodies showed endplate sclerosis, but the skull was spared. The ribs were somewhat broad and sclerotic. The metaphyses of the long and short tubular bones of the mice were all severely sclerotic and undermodelled, while the bone density of the diaphyses was decreased (see online supplementary table S4). Histology of the growth plate of the *Lrrk1* KO mice showed an elongated hypertrophic zone and delayed replacement of cartilage by bone (see online supplementary figure S2), corresponding to the metaphyseal changes seen on the radiographs. The close phenotypic resemblances between P1 and the *Lrrk1* KO mouse suggested that the deletion in P1 is a hypomorphic mutation that causes OSMD in humans.

Functional analysis of the *LRRK1* mutation

To test the lentiviral titre and expression levels of the FLAG-tagged *LRRK1* proteins, we transduced 293T cells with lentiviral particles at 5 MOI and extracted the total cellular protein. 293T cells can be easily transduced. We typically obtain 95% or greater transduction efficiency at 5 MOI. We tried different dosages of MOI in primary osteoclast precursors and found that at >5 MOI, some cells began to die after transduction. Therefore, we maintained 5 MOI for primary osteoclast precursors for osteoclast differentiation assays. An aliquot of the cellular protein was used for a western blot with an antibody against FLAG tag. The cells infected with lentivirus expressed comparable levels of wild-type and mutant *LRRK1* proteins (figure 4A). The transduction efficiency of lentiviral particles in primary cultures of monocytes derived from *Lrrk1* KO mice was >70% (figure 4B). To examine the function of the mutant *LRRK1*, osteoclast precursors from *Lrrk1* KO mice were infected with lentiviral particles expressing GFP (control), wild-type *LRRK1* or mutant *LRRK1*. Normal numbers of osteoclasts were generated in the KO and wild-type mice. The areas of mature TRAP-positive osteoclasts on bone slices were comparable for Lrrk1-deficient osteoclasts expressing GFP, wild-type *LRRK1* and mutant *LRRK1*. However, while the wild-type *LRRK1* in *Lrrk1*-deficient cells completely rescued the defect in osteoclast resorption activity, the mutant *LRRK1* failed to restore the osteoclast activity (figure 4C). There was no significant change in pit areas in the cells expressing mutant *LRRK1* as compared with that expressing GFP. The area of resorption pits was reduced by 90% in Lrrk1-deficient GFP expressing cells as compared with that of the wild-type cells (figure 4D). The individual resorption pits remained smaller and the pits were shallower in the mutant *LRRK1*-expressing osteoclasts. These data strongly suggest that the mutation has a hypomorphic effect on the function of *LRRK1*.

Screening of *LRRK1* mutation in P2 and P3

We checked the coverage of the exome sequence data for P2 and examined all exons that had low coverage (<96%) by Sanger sequencing; however, we found no variants likely to be

disease causing. In P2 who was a child of consanguineous parents, we found some heterozygous variants in *LRRK1*, and homozygosity mapping using the exome data showed no long homozygous stretch containing *LRRK1*. These results suggest that P2 is unlikely to have a *LRRK1* mutation. We also Sanger sequenced P3 for all *LRRK1* exons and flanking introns, but found no *LRRK1* mutation.

DISCUSSION

The identification of a biallelic and hypomorphic *LRRK1* mutation in a boy with radiographic features of OSMD indicates that this gene plays a role in bone homoeostasis in humans. This assumption is reinforced by the observation that *Lrrk1* KO mice exhibit a similar radiographic phenotype with dense and broad osteosclerotic bands in the metaphyses of tubular bones (figures 2 and 3, see online supplementary table S4). In addition, the growth plate abnormalities in these mice with expanded hypertrophic zone and delayed endochondral ossification (see online supplementary figure S2) may explain the shortness in the affected boy and KO mice. The osteopetrotic changes in the mouse result from markedly delayed resorption of cartilage matrices owing to dysfunction of mature osteoclasts. While *Lrrk1* expression is very low in murine osteoblasts and osteocytes compared with osteoclasts (see online supplementary figure S3), its expression is increased in osteoclasts in the late stage of differentiation (see online supplementary figure S4), suggesting a role of *Lrrk1* in the maturation of multinucleated osteoclasts. Consistently, *Lrrk1* KO mice show osteoclast-rich osteopetrosis due to the dysfunction of multinucleated osteoclasts.[19] Osteoclast precursors derived from *Lrrk1* KO mice differentiate into multinucleated cells in response to M-CSF and RANKL treatment, but these cells cannot form peripheral sealing zones and ruffled borders and hence experience difficulties in resorbing bone.[19] This defect of osteoclast function is partially rescued by overexpression of the constitutively active form of c-Src (Y527F). Immunoprecipitation assays in osteoclasts showed a physical interaction of *Lrrk1* with the C-terminal end of Src kinase (Csk).[19]

We could not identify a *LRRK1* mutation in P2 and P3. P2 is one of the original patients reported with OSMD.[2] We examined both patients for the entire coding exons of *LRRK1* and their surrounding introns by, respectively, exome sequencing and Sanger sequencing, but found no pathogenic nucleotide change. Although P2 is a child of consanguineous parents, homozygosity mapping using the exome data showed that *LRRK1* is not residing in a homozygous stretch. In addition, Sanger sequencing of *LRRK1* revealed several heterozygous SNPs in P2. These data suggest that OSMD is a genetically heterogeneous condition and that other genes must also be responsible for this rare disorder. The heterogeneity of OSMD is also reflected by the observation that P1 did not have raised ALP, although this has been described in the original patients. Interestingly, the *Lrrk1* KO mice have decreased ALP levels. The differences in ALP levels in OSMD may indicate that the causal genes interfere at different stages in osteoclastogenesis and/or osteoclast function.

Our data provide new insights into the pathophysiology of increased bone mass phenotypes and also may provide us with new opportunities for the treatment of osteoporosis, one of the most serious health problems in the elderly.[20] Understanding the genetic defects causing pycnodysostosis (OMIM: 265800) and sclerosteosis (OMIM: 269500) has resulted in the

development of good drug targets for osteoporosis, exemplified by the use of inhibitors for cathepsin K and ClC-7 and of anti-sclerostin antibodies.[21–23] It is of note that bone mineral density of *Lrrk1* KO mouse is the highest among 3629 distinct KO mouse lines, including *Sost* and *c-Src* KO mice.[19] *LRRK1* would therefore be a good target molecule for the treatment of osteoporosis. The KO mice have lifelong accumulation of bone; the age-related bone loss does not seem to occur in these mice, as trabecular bone mineral density measurements remain stable across ages. The mice also respond normally to the anabolic actions of teriparatide treatment and are resistant to ovariectomy-induced bone loss, the model of postmenopausal osteoporosis.[19] These findings suggest that *LRRK1* may be a fascinating new drug target that is specific to osteoporosis and has few or no side effects during long-term treatment.

Supplementary Material

Refer to Web version on PubMed Central for supplementary material.

Acknowledgments

We thank the patients and their families for their help with the study. We also thank N Atsumi for checking the English. The Department of Veterans Affairs in Loma Linda, California provided facilities to carry out the *Lrrk1* knockout mouse work.

Funding

This study was supported by research grants from the Japan Agency For Medical Research and Development (AMED) (contract No 14525125) and by the European Commission Seventh Framework Programme (SYBIL project; grant number 602300). WX was supported by grant 1R21 AR066831-01 from the National Institutes of Health and a GAP (Grants in Aid Program) grant from the American Society for Bone and Mineral Research. ZW was supported by Takeda Science Foundation, Japan.

References

1. Warman ML, Cormier-Daire V, Hall C, Krakow D, Lachman R, Lemerrer M, Mortier G, Mundlos S, Nishimura G, Rimoin DL, Robertson S, Savarirayan R, Sillence D, Spranger J, Unger S, Zabel B, Superti-Furga A. Nosology and classification of genetic skeletal disorders: 2010 revision. Am J Med Genet A. 2011; 155A:943–68. [PubMed: 21438135]
2. Nishimura G, Kozlowski K. Osteosclerotic metaphyseal dysplasia. Pediatr Radiol. 1993; 23:450–2. [PubMed: 8255649]
3. Mennel EA, John SD. Osteosclerotic metaphyseal dysplasia: a skeletal dysplasia that may mimic lead poisoning in a child with hypotonia and seizures. Pediatr Radiol. 2003; 33:11–14. [PubMed: 12497229]
4. Kasapkara CS, Kucukcongar A, Boyunağa O, Bedir T, Oncü F, Hasanoglu A, Tumer L. An extremely rare case: osteosclerotic metaphyseal dysplasia. Genet Couns. 2013; 24:69–74. [PubMed: 23610867]
5. Zheng H, Cai J, Wang L, He X. Osteosclerotic metaphyseal dysplasia with extensive interstitial pulmonary lesions: a case report and literature review. Skeletal Radiol. 2015; 44:1529–33. [PubMed: 26084987]
6. Nakajima M, Mizumoto S, Miyake N, Kogawa R, Iida A, Ito H, Kitoh H, Hirayama A, Mitsubuchi H, Miyazaki O, Kosaki R, Horikawa R, Lai A, Mendoza-Londono R, Dupuis L, Chitayat D, Howard A, Leal GF, Cavalcanti D, Tsurusaki Y, Saitsu H, Watanabe S, Lausch E, Unger S, Bonafé L, Ohashi H, Superti-Furga A, Matsumoto N, Sugahara K, Nishimura G, Ikegawa S. Mutations in B3GALT6, which encodes a glycosaminoglycan linker region enzyme, cause a spectrum of skeletal and connective tissue disorders. Am J Hum Genet. 2013; 92:927–34. [PubMed: 23664117]

7. Nakajima J, Okamoto N, Tohyama J, Kato M, Arai H, Funahashi O, Tsurusaki Y, Nakashima M, Kawashima H, Saitsu H, Matsumoto N, Miyake N. De novo EEF1A2 mutations in patients with characteristic facial features, intellectual disability, autistic behaviors and epilepsy. Clin Genet. 2015; 87:356–61. [PubMed: 24697219]
8. Miyatake S, Tada H, Moriya S, Takanashi J, Hirano Y, Hayashi M, Oya Y, Nakashima M, Tsurusaki Y, Miyake N, Matsumoto N, Saitsu H. Atypical giant axonal neuropathy arising from a homozygous mutation by uniparental isodisomy. Clin Genet. 2015; 87:395–7. [PubMed: 25040701]
9. Hayashi M, Nakashima T, Taniguchi M, Kodama T, Kumanogoh A, Takayanagi H. Osteoprotection by semaphorin 3A. Nature. 2012; 485:69–74. [PubMed: 22522930]
10. Kelly NH, Schimenti JC, Patrick Ross F, van der Meulen MCH. A method for isolating high quality RNA from mouse cortical and cancellous bone. Bone. 2014; 68:1–5. [PubMed: 25073031]
11. Nakashima T, Hayashi M, Fukunaga T, Kurata K, Oh-hora M, Feng JQ, Bonewald LF, Kodama T, Wutz A, Wagner EF, Penninger JM, Takayanagi H. Evidence for osteocyte regulation of bone homeostasis through RANKL expression. Nat Med. 2011; 17:1231–4. [PubMed: 21909105]
12. Xing W, Kim J, Wergedal J, Chen ST, Mohan S. Ephrin B1 regulates bone marrow stromal cell differentiation and bone formation by influencing TAZ transactivation via complex formation with NHERF1. Mol Cell Biol. 2010; 30:711–21. [PubMed: 19995908]
13. Cheng S, Zhao SL, Nelson B, Kesavan C, Qin X, Wergedal J, Mohan S, Xing W. Targeted disruption of ephrin B1 in cells of myeloid lineage increases osteoclast differentiation and bone resorption in mice. PLoS ONE. 2012; 7:e32887. [PubMed: 22403721]
14. Korr D, Toschi L, Donner P, Pohlenz HD, Kreft B, Weiss B. *LRRK1* protein kinase activity is stimulated upon binding of GTP to its Roc domain. Cell Signal. 2006; 18:910–20. [PubMed: 16243488]
15. Civiero L, Bubacco L. Human leucine-rich repeat kinase 1 and 2: intersecting or unrelated functions? Biochem Soc Trans. 2012; 40:1095–101. [PubMed: 22988872]
16. Bosgraaf L, Van Haastert PJ. Roc, a Ras/GTPase domain in complex proteins. Biochim Biophys Acta. 2003; 1643:5–10. [PubMed: 14654223]
17. Marín I. The Parkinson disease gene LRRK2: evolutionary and structural insights. Mol Biol Evol. 2006; 23:2423–33. [PubMed: 16966681]
18. Stirnimann CU, Petsalaki E, Russell RB, Müller CW. WD40 proteins propel cellular networks. Trends Biochem Sci. 2010; 35:565–74. [PubMed: 20451393]
19. Xing W, Liu J, Cheng S, Vogel P, Mohan S, Brommage R. Targeted disruption of leucine-rich repeat kinase 1 but not leucine-rich repeat kinase 2 in mice causes severe osteopetrosis. J Bone Miner Res. 2013; 28:1962–74. [PubMed: 23526378]
20. Harvey, N., Earl, S., Cooper, C. Epidemiology of osteoporotic fractures. In: Favus, MJ., editor. Primer on the metabolic bone diseases and disorders of mineral metabolism. 6th. USA: American Society for Bone & Mineral; 2006. p. 244-8.
21. Gallagher JA, Ranganath LR, Boyde A. Lessons from rare diseases of cartilage and bone. Curr Opin Pharmacol. 2015; 22:107–14. [PubMed: 25978274]
22. Henriksen K, Thudium CS, Christiansen C, Karsdal MA. Novel targets for the prevention of osteoporosis—lessons learned from studies of metabolic bone disorders. Expert Opin Ther Targets. 2015; 19:1575–84. [PubMed: 25960169]
23. Fijalkowski I, Boudin E, Mortier G, Van Hul W. Sclerosing bone dysplasias: leads toward novel osteoporosis treatments. Curr Osteoporos Rep. 2014; 12:243–51. [PubMed: 24947952]

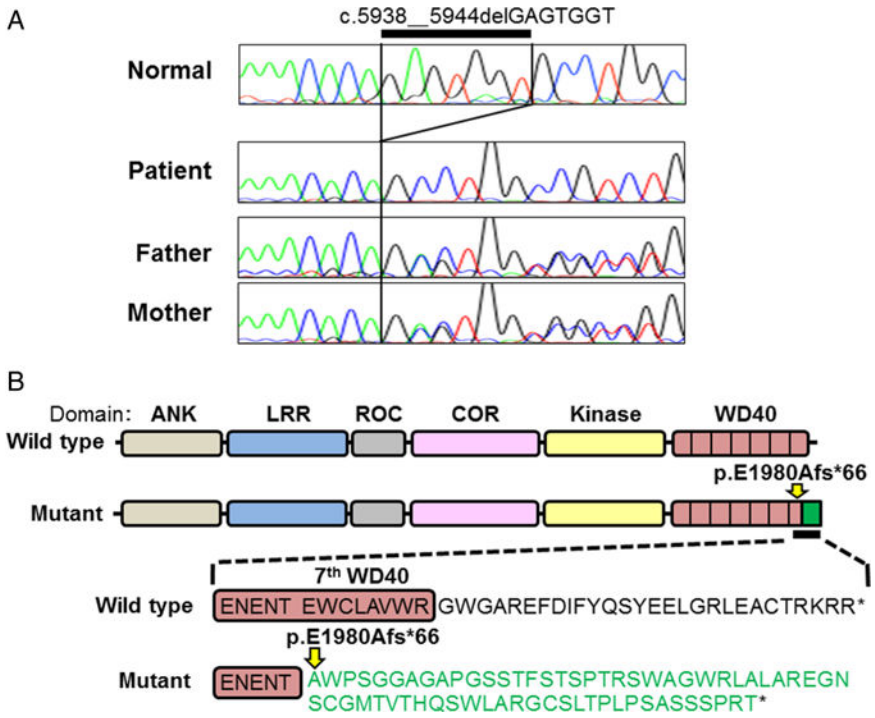

Figure 1.

LRRK1 mutation in patient 1. (A) Electropherograms in family 1. Homozygous deletion (c. 5938-5944delGAGTGGT) in the patient (P1). The parents are heterozygous for the deletion. (B) *LRRK1* protein structure and location of the mutation. The mutation causes a frame-shift within the seventh WD40 domain in the C-terminus of the *LRRK1* protein. The additional 66 amino acids in the mutated protein are shown by a green box and green letters.

Figure 2.

Radiographs of patient 1 at age 14 months. (A) Skull anteroposterior (A-P). Normal skull. (B) Lateral spine. No platyspondyly. Ribs are broad. (C) Left hand A-P. Broad and sclerotic metaphyses in the distal radius and ulna. Sclerotic metaphyses of metacarpals and phalanges. (D) Pelvis A-P. Marginal sclerosis of the ilia. Broad and sclerotic metaphyses of the proximal femur.

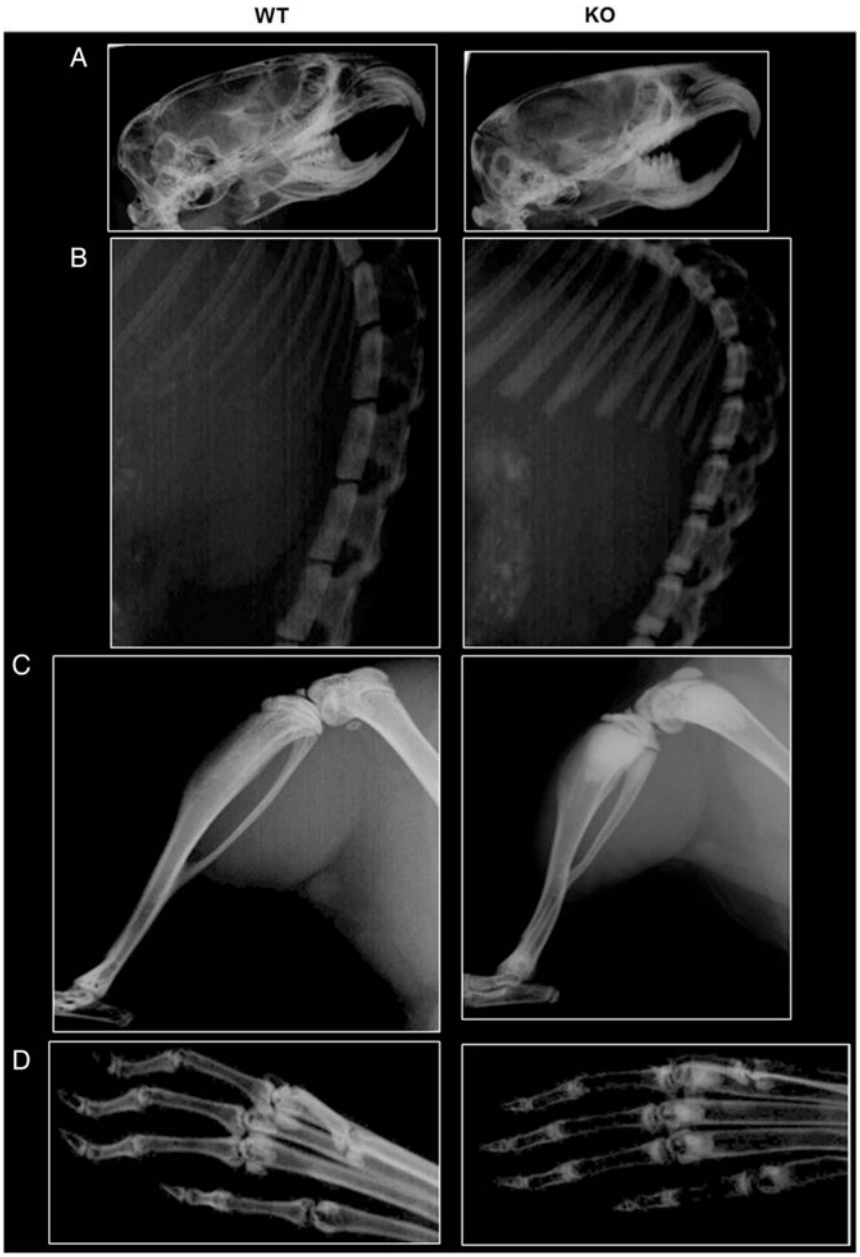

Figure 3.

Radiographs of the *Lrrk1* knock-out (KO) mouse at 8 weeks compared with the wild-type (WT). (A) Skull. There is no difference in the bone density of the skull and teeth. (B) The height of the vertebral bodies of the KO mouse is decreased with marginal sclerosis and the ribs are broad and sclerotic. (C) Lower leg. In the KO mouse, the metaphyses of the long tubular bones are severely sclerotic and undermodelled. There is also shortening of the long bones. (D) Feet. In the KO mouse, the metaphyses of the short tubular bones are sclerotic and undermodelled, while the bone density of the diaphyses is decreased.

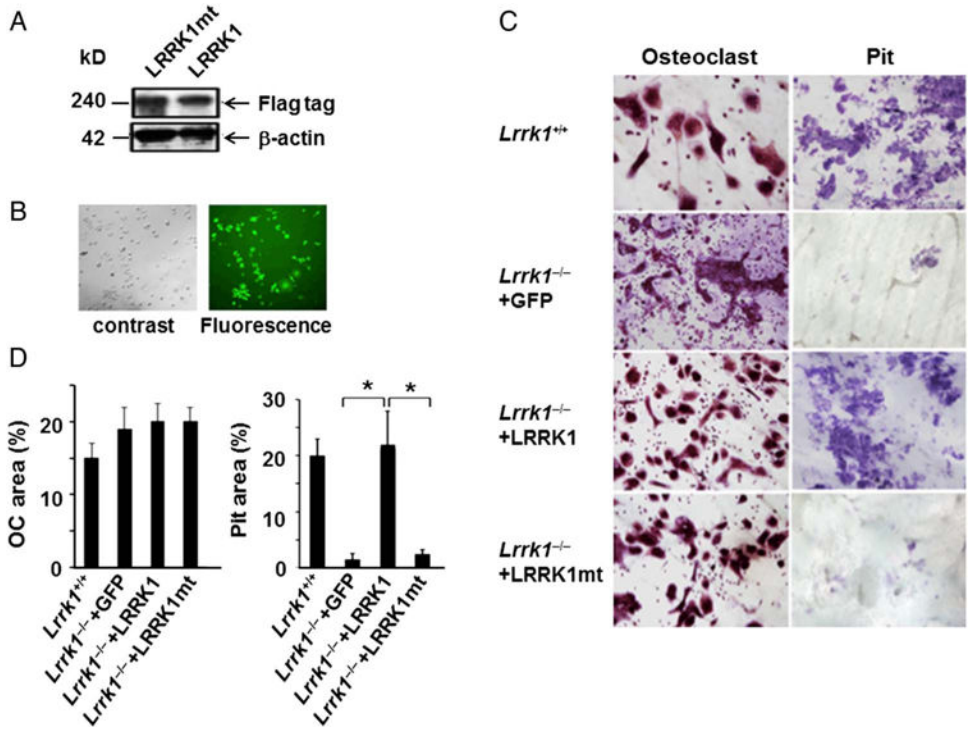

Figure 4.

Overexpression of the *LRRK1* mutant protein does not rescue bone resorption defect of *Lrrk1*-deficient osteoclasts. (A) Comparable expression of FLAG-tagged wild-type (*LRRK1*) and mutant (*LRRK1*mt: p.E1980Afs*66) human *LRRK1* proteins. 293T cells were infected with lentiviral particles and cultured in fresh medium for 12–36 h after infection. Total cellular extracts were subjected to western blot using anti-FLAG antibody. (B) Efficient transduction of lentiviral particle in osteoclast precursors. Primary monocytes derived from the spleen of *Lrrk1* knockout mice were seeded in 48-well plates containing bone slices and infected with lentiviral particles. The transduction efficiency is monitored by green fluorescent protein (GFP) expression in the cells that grow at the edges of bone slices 48 h after transduction. (C) Tartrate-resistant acid phosphatase (TRAP)-positive osteoclasts and resorptive pit formation on bone slices (×100). Left panel: lentivirus transduced monocytes were differentiated on bone slices for 6 days, followed by TRAP staining. Right panel: transduced monocytes in another 48-well plate were differentiated on bone slices for 10 days. The cells were removed and pits were stained with haematoxylin. (D) Quantitative data of TRAP-positive multinuclear cells (left) and pit formation (right) from three independent experiments, with three bone slices each time (N=9). Data are the means±SEM and analysed using Student’s t test. *$p<0.01$.